# Ultrafast Dynamics of Porphyrins in the Condensed Phase: I. Free Base Tetraphenylporphyrin†

**J. Spencer Baskin, Hua-Zhong Yu,‡ and Ahmed H. Zewail***

*Laboratory for Molecular Sciences, Arthur Amos Noyes Laboratory of Chemical Physics, California Institute of Technology, Pasadena, California 91125*

*Received: February 11, 2002; In Final Form: April 17, 2002*

With femtosecond resolution, using fluorescence up-conversion and transient absorption, we have carried out measurements on free base tetraphenylporphyrin ($H_2$TPP) in benzene solution, pumping with ∼1300 $cm^{-1}$ of excess vibrational energy in each of the Soret, $Q_y$, and $Q_x$ bands, and also pumping the lowest vibrational band of $Q_y$. From these studies, made for different excitations and at different detection wavelengths, we provide a model for describing the elementary intramolecular processes in the Soret, $Q_y$, and $Q_x$ electronic manifolds, with the following order of time scales and couplings: electronic (femtosecond), vibrational (femtosecond−picosecond), and singlet−triplet (nanosecond). These dynamical electronic and vibrational relaxation pathways in a molecule with small dipole in nonpolar solvents can be studied without interference from solvent reorganization, as indicated by the small Stokes shift of fluorescence. Vibrationally excited Soret → $\{Q_y,Q_x\}$ and $Q_y \rightarrow Q_x$ electronic relaxation occurs in less than 100 fs, within our resolution, as evidenced by the immediate rise of $Q_x$ fluorescence after Soret (397 nm) and $Q_y$ (514 and 550 nm) excitation. There are generally three distinguishable ultrafast relaxation time scales within the $Q_x$ state, which are assigned to intra- and intermolecular vibrational relaxation processes leading to thermal equilibrium in $Q_x$, the lowest excited singlet state. The measured time scales are as follows: 100−200 fs for intramolecular vibrational energy redistribution, 1.4 ps for vibrational redistribution caused by elastic collision with solvent molecules, and 10−20 ps for thermal equilibration by energy exchange with the solvent. Decay of the equilibrated $Q_x$ population occurs on the nanosecond time scale by intersystem crossing to the triplet state.

## 1. Introduction

Porphyrins are a class of molecules with key roles in many important biological processes and, as such, are at the focus of a wide variety of research efforts, from fundamental studies of their chemical versatility and photophysical properties to practical exploration of their photosynthetic and catalytic functions.[1,2] A detailed understanding of electronic and vibrational relaxation of excited porphyrins and the influence of the solvent and of the wide array of commonly encountered peripheral substituents and metal centers is an important goal of much recent work in the field.[3−8]

Our interest in the relaxation dynamics of porphyrins is an outgrowth of femtosecond studies[9−11] aimed at elucidating the novel electrocatalytic properties of a class of ruthenated cobalt porphyrins.[12] Zinc and free base analogues were chosen to serve as reference systems to establish which observations could be uniquely attributed to the presence of cobalt and particularly to changes in electronic structure due to cobalt's unpaired d electron. When these non-cobalt systems were found to undergo ultrafast dynamic processes as yet not clearly understood, we continued with a systematic investigation. Not only are these systems of great interest in their own right, but a clear understanding of porphyrin excited-state relaxation dynamics in the absence of cobalt may also prove important to interpretation of the ultrafast dynamics observed in the catalytic systems.

The purpose of this and the following paper[13] is to provide a detailed picture of the relaxation dynamics in the $S_2$ and $S_1$ states of free base tetraphenylporphyrin ($H_2$TPP) and zinc tetraphenylporphyrin (ZnTPP), respectively. Both systems show a wide range of dynamic time scales but are fundamentally and strikingly dissimilar in the details of their relaxation processes. Because interference from a substantial dynamic solvation effect is not expected for a solute with small or zero dipole in nonpolar solvent, both are very well-suited to experimental characterization of the vibrational relaxation process in solution, which is currently a topic of great interest.[14] Evidence of the minor role of dynamic solvation upon excitation of $H_2$TPP and ZnTPP can be seen in the small Stokes shift of their respective static fluorescence spectra.

The absorption and emission spectroscopy of free base tetraphenylporphyrin ($H_2$TPP) has been thoroughly characterized,[1,15−18] with measurement of the ground-state absorption spectrum of $H_2$TPP in benzene first reported over 50 years ago.[15] The nanosecond lifetime of $Q_x$, the lowest excited singlet state ($S_1$), and microsecond lifetime of the lowest triplet state ($T_1$) have also been measured.[19−21] Ultrafast study of $H_2$TPP has not been extensive, however. One study employing femtosecond fluorescence depletion[22] has been interpreted to indicate an $S_2$ lifetime of $H_2$TPP in chloroform of a few tens of femtoseconds[22] or 200 fs,[23] a result consistent with the low $S_2$ fluorescence yield of free base porphyrins compared to metalloporphyrins.[24,25] Paradoxically, however, line widths measured of the distinct and sharp lines in the absorption spectrum of supersonically cooled, isolated $H_2$TPP molecules indicate a lifetime at the $S_2$ electronic origin of at least 5 ps.[26]

† Part of the special issue "Jack Beauchamp Festschrift".

* To whom correspondence should be addressed.

‡ Present address: Department of Chemistry, Simon Fraser University, Burnaby, British Columbia V5A 1S6, Canada.

10.1021/jp020398g CCC: $22.00 
Published on Web 08/03/2002

We have carried out measurements on $H_2TPP$ in benzene solution exciting the Soret band, vibrationally excited and vibrationless levels of $Q_y$, and vibrationally excited $Q_x$. These show internal conversion from the higher electronic states to $Q_x$ occurring within ~50 fs. The rapid flow of population into vibrationally excited levels of $Q_x$ is followed by three distinct ultrafast processes of intramolecular vibrational energy redistribution, elastic-collision-induced vibrational energy redistribution, and vibrational relaxation to reach thermal equilibrium in the long-lived $Q_x$ state.

## 2. Experimental Section

**Apparatus and Procedures.** Femtosecond fluorescence up-conversion and transient absorption measurements were performed in the Laboratory for Molecular Sciences facility at Caltech, of which brief descriptions have been given previously.[9,27] For both techniques, the output of an amplified titanium−sapphire laser system (Spectra-Physics Tsunami/Spitfire, producing 80 fs pulses at a 1 kHz repetition rate with pulse energies of 2 mJ near 800 nm) was split into equal parts to generate the pump and probe pulse trains. For the pump, one-half of the fundamental light was either doubled for excitation in the Soret band or used to pump an optical parametric amplifier (OPA), the IR output of which was mixed with the residual fundamental to provide wavelengths between 514 and 590 nm. The pump pulse passed through a computer-controlled optical delay line and was focused by a 30 cm focal length lens. The sample cell was typically displaced several inches from the focus to give an excitation spot size of ~450 $\mu$m. Pump power was varied from 0.07 $\mu$J/pulse to 3.5 $\mu$J/pulse to study the power dependence of the measured dynamics.

In fluorescence up-conversion experiments, fluorescence from the excited sample was collected and focused by two parabolic mirrors into a 1 mm thick BBO crystal. Color filters were placed between the mirrors to reject scattered laser light and pass the desired fluorescence wavelengths, ranging from 415 to 720 nm. The probe half of the fundamental beam, attenuated to 10−50 $\mu$J/pulse, was overlapped noncollinearly with the fluorescence in the BBO crystal to allow generation of sum-frequency radiation between 273 and 379 nm. After the crystal, the up-converted signal was spatially separated from the fundamental beam, focused on the entrance slit of a 0.25 m monochromator, and detected by a photomultiplier at the exit slit. Up-conversion at the selected wavelength (±3 nm) was maximized by angle tuning the BBO crystal. A UG11 filter and, when needed, a cell of neat benzene were placed before the monochromator entrance slit to cut background signals from, respectively, the second harmonic (~400 nm) and third harmonic (~266 nm) of the probe beam generated in the mixing crystal. The linear polarization of the pump beam was set at 54.7° to the mixing axis of the crystal to eliminate the influence of induced sample anisotropy on the fluorescence signal. The photomultiplier output was integrated by a gated integrator (SR250) and recorded as a function of pump−probe time delay.

For transient absorption measurements, the probe half of the fundamental was used to pump a second OPA. Probe wavelengths from 470 to 702 nm were produced by mixing or doubling the parametrically amplified IR light. Typical probe pulse energies used were from 0.01 to 0.5 $\mu$J at the sample. A beam-splitter separated a small fraction of the probe beam for measurement by a photodiode before the probe crossed the pump beam at a small angle (~3°) in the sample cell, with the angle between pump and probe polarizations set at 54.7°. To determine the change in absorbance, $\Delta A$, at the probe wavelength as a result of the pump excitation, a chopper was placed in the pump beam and the probe energy after traversing the sample was measured by photodiode in the presence and absence of pump pulse excitation. The photodiode signals were integrated by an SR250, transferred to a computer, and normalized to the probe energy measured before the sample cell. The negative logarithm of the ratio between these normalized probe signals, recorded as a function of the time delay between passage of the pump and probe pulses, constituted the $\Delta A$ transients. Two probe detection modes were employed, both ensuring the suppression of anisotropy effects. Either the entire probe pulse was focused on one photodiode, or the pulse was analyzed into polarization components parallel and perpendicular to the pump polarization, and the energies of the components were measured separately. In the latter mode, the isotropic $\Delta A$ ($\equiv \Delta A_{54.7}$) was reconstructed as the sum $\Delta A_{\parallel} + 2\Delta A_{\perp}$.

For best temporal resolution and to minimize the signal from solvent alone, experiments to investigate subpicosecond dynamics were performed in fused silica cells with 1 mm sample path lengths. Comparison scans of cells containing pure solvent were recorded in conjunction with experiments under those conditions for which interference from solvent-induced transients was observed to be potentially significant. To use small quantities of the samples and still avoid extended irradiation of a fixed volume, the 1 mm cells were translated across the light path periodically during most measurements. When longer time behavior was the focus, cells with 5 mm path lengths were normally used, and the samples were stirred.

The measured signals for both up-conversion and transient absorption were analyzed by fitting to a sum of exponential terms, $S(t) = \sum A_i \exp(-t/\tau_i)$, with independent amplitudes, $A_i$, and lifetimes, $\tau_i$, using the minimum number of components required to leave no systematic deviation of the residual. Convolution with a Gaussian response function was included in the fitting procedure. The total temporal response of the system for experiments in cells of 1 mm path length typically ranged from 250 to 350 fs for transient absorption and 350 to 550 fs for fluorescence.

Ground-state absorption and static fluorescence spectra were obtained by using a UV−vis spectrometer (Cary, 50 Conc) and a fluorometer (ISA, FluoroMax-2). Absorption spectra were recorded initially to confirm the quality of each sample prepared for use in femtosecond measurements and periodically to check for degradation over time.

**Materials.** The $H_2TPP$ molecule was prepared and purified as described previously.[9] Benzene (EM Science, OmniSolv) was passed through a column of aluminum oxide (Aldrich, activated, basic, Brockmann I) before use. All experiments were carried out on aerated samples at ambient temperature (~24 °C).

## 3. Results

**Preliminary.** In Figure 1 are shown ground-state absorption and fluorescence spectra of $H_2TPP$ in benzene. In the absorption spectrum, the Soret or B band has a single peak at 419 nm with a shoulder at ~401 nm. The Q band, which is degenerate in the $D_{4h}$ symmetry of metalloporphyrins, splits because of the lower symmetry of $H_2TPP$ into two components of unequal energy, $Q_x$ and $Q_y$, with five distinct peaks.[15−18] The strongest of these is at 514 nm and assigned as $Q_y(1,0)$, where the numbers in parentheses indicate the number of quanta of the dominant Franck−Condon active vibrational mode in the upper and lower electronic states of the transition, respectively. Additional peaks assigned as $Q_y(2,0)$, $Q_y(0,0)$, $Q_x(1,0)$, and $Q_x(0,0)$ are found at 483, 549, 592, and 647 nm. The positions of all absorption peaks

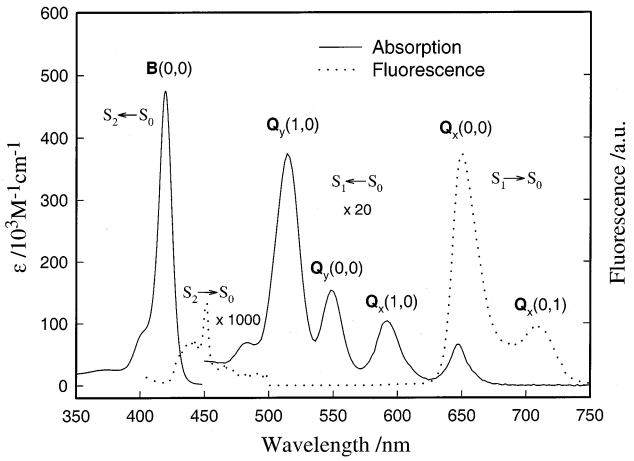


**Figure 1.** The ground-state absorption and static fluorescence spectra of $H_2TPP$ in benzene. For the fluorescence spectrum, the excitation wavelength was 397 nm. At the sample concentration of ~4 $\mu$M in a 5 mm cell, reabsorption may be significant below 430 nm. The fluorescence intensity at wavelengths longer than 680 nm is not very accurate; see text.

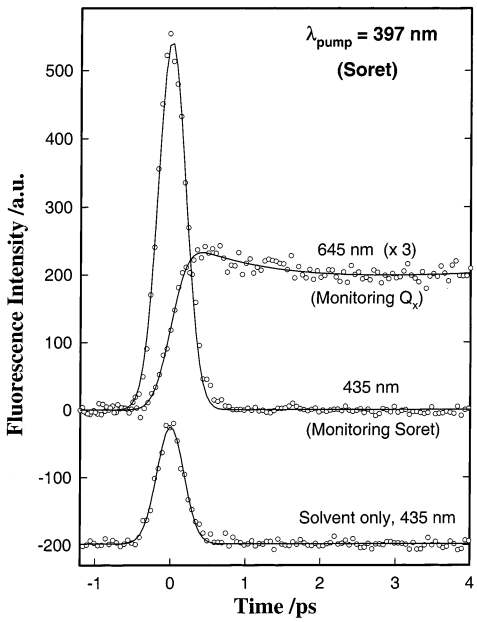


**Figure 2.** Fluorescence transients of $H_2TPP$ in benzene at 435 and 645 nm with excitation of 0.9 $\mu$J/pulse at 397 nm. The solvent response at 435 nm is shown, while no detectable (<5% of the $H_2TPP$ signal) peak was seen in pure benzene for measurement at 645 nm. The intensity scale has been normalized to correspond to equal excited populations, because the 645 nm experiment was done at higher sample concentration ($A_{397}$ = 0.7 vs. 0.06). Solid lines are fits of the experimental data. The fit parameters for the 645 nm data are the same as those given for 650 nm in Table 1. The solvent response at 435 nm is fit to a Gaussian function of 426 fs fwhm, while the $H_2TPP$ transient at 435 nm is fit with a 426 fs response and a 29 fs decay.

are within ±2 nm of previously reported values.[16−18] The lowest triplet state, $T_1$, lies below the $Q_x$ state.

The dominant features of the fluorescence spectrum of Figure 1, for 397 nm excitation, are the $Q_x(0,0)$ and $Q_x(0,1)$ peaks, which we find at 650 and 709 nm. We note that this position of the latter peak, and its intensity in Figure 1, differ from those reported in refs 18 and 28, a discrepancy that may be due to inaccuracy in our correction for the detector sensitivity of the fluorometer used in this work, which drops off severely for wavelengths longer than 680 nm. Additionally, there is a broad shoulder centered at ~605 nm with amplitude <1% of that of the 650 nm peak. The fluorescence quantum yield of $H_2TPP$ in benzene at room temperature has been reported as 0.11[18,21] or 0.13,[28] and the lifetime of $Q_x(0,0)$ emission in the same solvent was measured by single photon counting to be 12.4 ns.[21] The dominant channel for $Q_x$ relaxation is intersystem crossing to $T_1$, and the lifetime of the $T_1$ state is milliseconds in degassed solvents.[19,20] Evidence of the minor role of dynamic solvation for excitation of $H_2TPP$ in benzene can be seen in the very small Stokes shift of the static fluorescence spectrum.

In previous studies of $H_2TPP$,[1,18,25] no Soret band fluorescence has been reported. Kobayashi and co-workers[21,25] measured Soret fluorescence from numerous metallotetraphenylporphyrins in a variety of solvents but were unable to detect it from $H_2TPP$. The Soret fluorescence of one free base porphyrin, tetrabenzoporphyrin ($H_2TBP$), was measured by Kotlo et al.[24] in several solvents. In pyridine solution, the ratio of Soret fluorescence to Q fluorescence was reported to be a factor of 20 smaller for $H_2TBP$ than for ZnTBP. If this ratio is typical, then the yield of $H_2TPP$ Soret fluorescence $\varphi^{S_2}$ in benzene may be expected to be less than $10^{-4}$, on the basis of those yields that have been measured for ZnTPP (B and Q bands) and $H_2TPP$ (Q band) in that solvent.[21]

In Figure 1, the emission detected below 500 nm has been amplified by a factor of 1000. The sharp feature at 451.5 nm, which is also seen in the pure solvent, corresponds to the unresolved 3047 and 3062 cm$^{-1}$ C−H stretch Raman peaks of benzene-$h_6$, but the broad band from 440 to 450 nm is due to $H_2TPP$. Because this emission is so weak, it could not be measured at very low $H_2TPP$ concentration to make the influence of reabsorption insignificant; therefore, Figure 1 cannot be taken as an accurate representation of the true Soret emission profile. (See ref 13 for a discussion of reabsorption in ZnTPP.) If, nonetheless, we integrate the measured intensities to estimate $\varphi^{S_2}/\varphi^{S_1}$, we can obtain an approximate value for $\varphi^{S_2}$ of $1 \times 10^{-5}$. If reabsorption is important, as expected, this value is a lower limit to $\varphi^{S_2}$. Given that the radiative lifetime of porphyrin Soret bands, based on the absorption oscillator strength and the Strickler−Berg formula,[29] is of the order of 1 ns,[25,30] the Soret fluorescence lifetime may be estimated to be of the order of 10 fs.

**Fluorescence Up-Conversion Measurements.** To follow in real time the relaxation processes taking place in the excited states of $H_2TPP$, fluorescence transients were recorded with our fluorescence up-conversion apparatus for a number of different excitation and emission wavelengths. In Figure 2, we compare the temporal profiles of fluorescence from the Soret and $Q_x$ bands following excitation of the Soret band at 397 nm. The Soret emission was monitored at 435 nm, in the window between the benzene Raman band and the onset of strong reabsorption. The benzene response could not be completely avoided, as shown, but a signal enhancement from $H_2TPP$ was consistently seen, in accord with the observation of Soret fluorescence in the static emission spectrum. As seen in Figure 2, the temporal profiles of the signals for benzene alone or for $H_2TPP$ in benzene were very similar. Not only is broadening or asymmetry of the fluorescence signal slight, relative to the Raman peak, but the two are coincident in time (the measured delay of the fluorescence peak is 2 ± 10 fs with calibration for variations in dispersion of the individual cell windows).

For the same excitation, fluorescence monitored at the $Q_x(0,0)$ fluorescence band peak (645 nm) is seen in Figure 2 to appear within the apparatus temporal response. Subsequent evolution, on the picosecond and longer time scales, is also partially in evidence and will be considered below. The solvent response

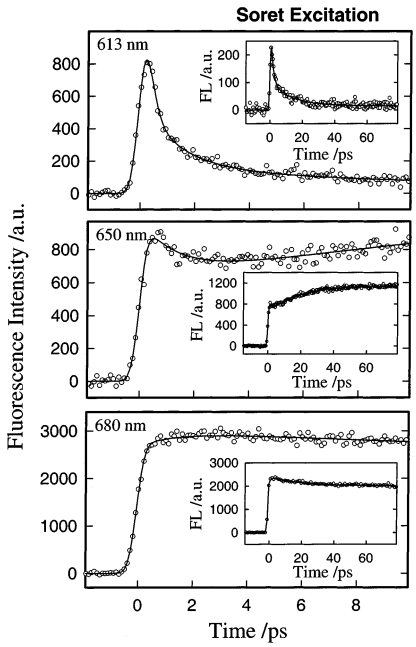


**Figure 3.** Comparison of fluorescence transients of $H_2TPP$ in benzene at the three wavelengths indicated for excitation at 397 nm (2 $\mu$J/pulse). The intensity scales are as measured. Solid lines are fits of the experimental data (see Table 1). The insets show the transient at longer time and lower time resolution (recorded in 5 mm cells). ($A_{397}$ for the six experiments ranged from 0.6 to 1.7).

measured at 645 nm indicates negligible solvent contribution to the measured $H_2TPP$ transient. When the benzene Raman peak at 435 nm is used as the system response function (422 fs fwhm), the 645 nm data fits perfectly with no initial rise time.

Figure 3 gives further examples of fluorescence transients measured across the $Q_x$ emission band, following Soret band excitation. The long-time data plotted as insets were recorded at lower time resolution so that the earliest features are not evident. At these and other detection wavelengths, the temporal evolution occurs on four distinct time scales, and in no case is an initial rise time clearly discernible. Although multiexponential fits of individual transients of this type allow only rather broad limits to be placed on component amplitudes and lifetimes, the need for at least four lifetimes is unambiguous, because four lifetimes are clearly seen in the single transient of 613 nm fluorescence. Furthermore, all fluorescence transients can be well fit using only lifetimes of the following values: 200 fs, 1.4 ps, 10−20 ps, and a lifetime that is too long to be measured accurately in our apparatus but is consistent with the $Q_x$ fluorescence lifetime of 12.4 ns.[21] The fit curves shown plotted with the data in Figure 3 were all constrained to use this set of lifetimes; all four are used at 613 nm, while three appear at the other two wavelengths, with amplitudes varying in size and sign. Component amplitudes resulting from the fitting of fluorescence transients at several different wavelengths are given in Table 1. The interpretation of the three femtosecond and picosecond lifetimes will be discussed later.

Fluorescence was also measured for excitation at 514 nm, the $Q_y(1,0)$ absorption band, and selected transients are shown in Figure 4 covering the entire wavelength range studied. Scaling of the plots shows true relative fluorescence intensities, based on comparison between the integrals of transient behavior and the static emission spectrum. For this and other excitations in the Q-band, effort was necessary to avoid substantial interference from solvent Raman peaks, and it proved helpful in this effort to use either benzene-$h_6$ or benzene-$d_6$ as solvent, depending

**TABLE 1: Component Relative Amplitudes of Fits of Fluorescence Up-Conversion Transients for 397 nm Excitation of $H_2TPP$ in Benzene**

| | relative amplitudes[a] | | | |
|---|---|---|---|---|
| $\lambda_{probe}$ (nm) | $A_1$ ($\tau_1 \equiv 0.2$ ps) | $A_2$ ($\tau_2 \equiv 1.4$ ps) | $A_3$ ($\tau_3 \equiv 10-20$ ps) | $A_4$ ($\tau_4 \equiv 12$ ns) |
| 572 | 0.8 | 0.15 | 0.04 | 0.006 |
| 600 | 0.7 | 0.25 | 0.04[b] | *b* |
| 613 | 0.7 | 0.2 | 0.1 | 0.01 |
| 650 | | 0.2 | −0.4 | 0.8 |
| 680 | | −0.1 | 0.2 | 0.8 |

[a] A negative amplitude indicates that the respective component is a rise instead of a decay. [b] Because no long time scan was recorded at 600 nm, only the total contribution $A_3 + A_4 = 0.04$ could be estimated.

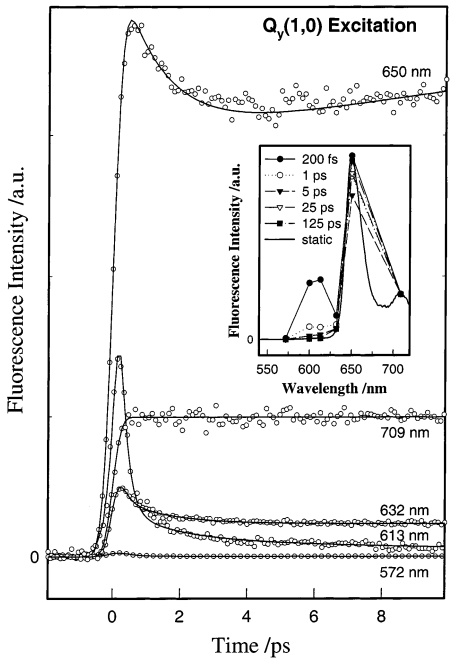


**Figure 4.** Comparison of fluorescence transients of $H_2TPP$ for excitation at 514 nm ($A_{514}$ ranged from 0.4 to 0.9, and pulse energies were between 1.5 and 2.5 $\mu$J) with detection wavelengths as indicated in the figure. The amplitudes are normalized to indicate the respective intensities in the static fluorescence spectrum of Figure 1. Benzene-$h_6$ was used as solvent at 572 nm. At all other wavelengths, benzene-$d_6$ was used and solvent-only scans produced negligible signals. Solid lines are fits of the experimental data using a common set of lifetimes (see text or Table 1). The inset shows the time evolution of the emission spectrum based on deconvolution of fits of measurements at six wavelengths. Reliability of intensity normalization is limited to about a factor of 2 below 632 nm because of dependence on the small values of relative amplitude $A_4$, while it is limited to a similar degree at 632 nm by the rapid change in the static fluorescence intensity over the range of up-conversion wavelength uncertainty.

on the fluorescence wavelength measured. For example, benzene-$d_6$ was used for fluorescence to the red of 600 nm when exciting at 514 nm because the major benzene-$h_6$ Raman peak for this excitation is located at 610 nm, while the corresponding peak in benzene-$d_6$ is at 582 nm.

These transients in Figure 4 are remarkably similar in appearance to those obtained by pumping the Soret band, as seen by comparing with the data of Figure 3; indeed, all transients could be fit to the same set of four lifetimes, and, at a given detection wavelength, the transients have component relative amplitudes that are similar for the two excitations. In the inset to Figure 4 is plotted a representation of the evolution of the emission spectrum with time, at six different wavelengths, using the appropriate multiexponential fit functions deconvoluted

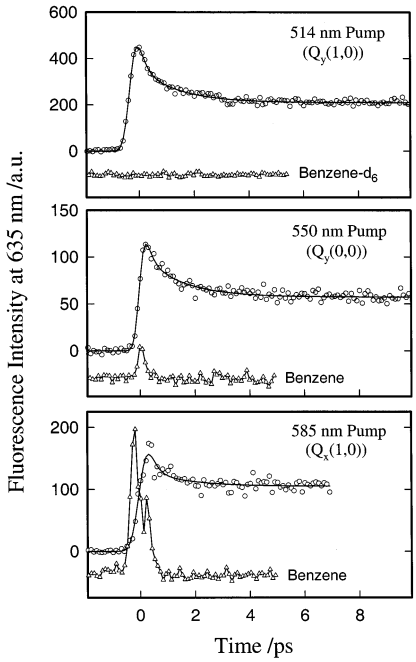


**Figure 5.** Comparison of 635 nm fluorescence of $H_2TPP$ for three excitation wavelengths. The solvent used in each experiment is indicated with the accompanying scan of a cell with that solvent alone. The laser energy and sample absorbance were as follows: (top) 1.6 $\mu$J/pulse, $A_{514} = 0.9$; (middle) 2.0 $\mu$J/pulse, $A_{550} = 0.5$; (bottom) 1.5 $\mu$J/pulse, $A_{585} = 0.25$. The intensity scales are as measured. Solid lines are fits of the experimental data using a common set of lifetimes (see text or Table 1).

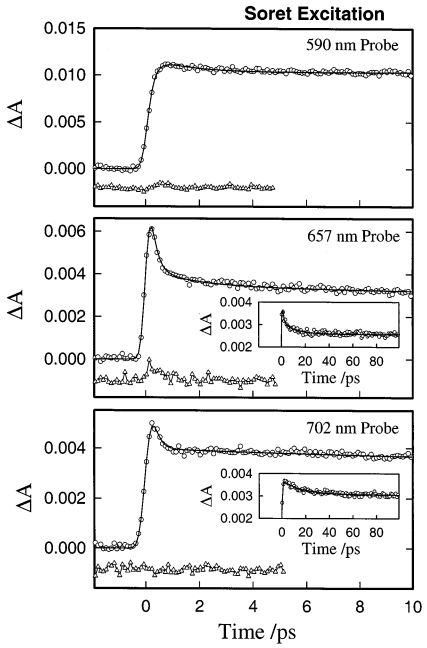


**Figure 6.** Femtosecond transient absorbance of $H_2TPP$ in benzene. Pump wavelength was 397 nm (2 $\mu$J/pulse); probe wavelengths were as shown. The short time data and associated solvent scans were recorded in 1 mm cells. The insets show transients at longer time and lower time resolution (recorded in 5 mm cells). $A_{397}$ was ~1.2 except for 657 nm probing, for which it was ~2.1. Solid lines are fits of the experimental data using a common set of lifetimes (see text or Table 1).

from the system temporal response. This plot makes it clear that from the earliest time resolvable with our apparatus the maximum emission intensity is measured at $Q_x(0,0)$. Thereafter, spectral narrowing occurs, most dramatically on the femtosecond time scale and continuing for tens of picoseconds, to reach the profile observed in static measurements.

Experiments were also carried out with excitation at $Q_y(0,0)$ (550 nm) and $Q_x(1,0)$ (585 nm), detecting fluorescence above 600 nm only. In Figure 5, fluorescence at 635 nm is compared for pumping three different Q-band levels. The signals from the pure solvent used in the respective measurement are shown below each transient. The signal when pumping $Q_y(0,0)$ is very similar to that for pumping $Q_y(1,0)$ and can be fit reasonably with the same lifetimes and similar amplitudes. The small solvent signal here does not constitute a substantial interference. In contrast, when pumping $Q_x(1,0)$ at 585 nm, a large solvent and surface scatter signal was always present at 635 nm, so the origin of the early time behavior of the transient for this pump wavelength is less clear-cut. The data do, however, indicate that the total amplitude of short decay components cannot be as large as when pumping $Q_y$ but also that some short component is likely still present, because a tail appears to reach beyond the range of possible solvent contamination.

**Transient Absorption Measurements.** Transient absorption measurements were also carried out, providing an alternate window with somewhat higher time resolution on the dynamics following excitation of the same four vibronic levels as studied by fluorescence up-conversion. In Figure 6 are shown the transients measured at three different probe wavelengths when pumping the Soret band. The associated solvent scans are plotted below each of the short-time transients, showing minimal solvent contribution. Again, four distinct components are required to fit all data sets, and the lifetimes correlate well with those used to fit the fluorescence transients. The fits plotted in Figure 6,

**TABLE 2: Component Relative Amplitudes of Fits of Transient Absorption Measurements for 397 nm Excitation of $H_2TPP$ in Benzene**

| | relative amplitudes[a] | | | |
|---|---|---|---|---|
| $\lambda_{probe}$ (nm) | $A_1$ ($\tau_1 \equiv 0.2$ ps) | $A_2$ ($\tau_2 \equiv 1.4$ ps) | $A_3$ ($\tau_3 \equiv 10-20$ ps) | $A_4$[b] |
| 590 | −0.6 | 0.15 | | 0.85 |
| 657 | 0.5 | 0.1 | 0.06 | 0.3 |
| 702 | 0.45 | | 0.1 | 0.45 |

[a] A negative amplitude indicates that the respective component is a rise instead of a decay. [b] $A_4$ is the amplitude of an effective component with lifetime greater than or equal to 12 ns, corresponding to both relaxed $Q_x$ and $T_1$ absorption.

for which the component relative amplitudes are given in Table 2, are those obtained by constraining the lifetimes to a common set of values. (Now, however, because $T_1$ absorption is comparable to that of $Q_x$ in the wavelength range probed,[31] the population dynamics for equilibrated $Q_x$ and $T_1$ are combined in an effective fourth component on our experimental time range. In the vicinity of 657 and 702 nm, for example, $Q_x$ and $T_1$ absorptions are approximately equal and the fourth lifetime becomes much longer than the 12 ns $Q_x$ lifetime.) All four lifetimes are evident probing at 657 nm, while three only are sufficient to fit the other two transients. Note that the 200 fs lifetime appears as a rise at 590 nm.

In Figure 7, the transient absorption at 657 nm is compared for three Q-band pump wavelengths, with solvent traces again displayed below the data. The transients for the two $Q_y$ excitations are very similar to each other. They are also similar to the 657 nm transient for 397 nm excitation, although the femtosecond component fits best to an even shorter lifetime for Q-band pumping (~110 fs) and the other components have slightly smaller amplitudes. When pumping $Q_x(1,0)$, the transient changes appearance, as was also the case for fluorescence up-

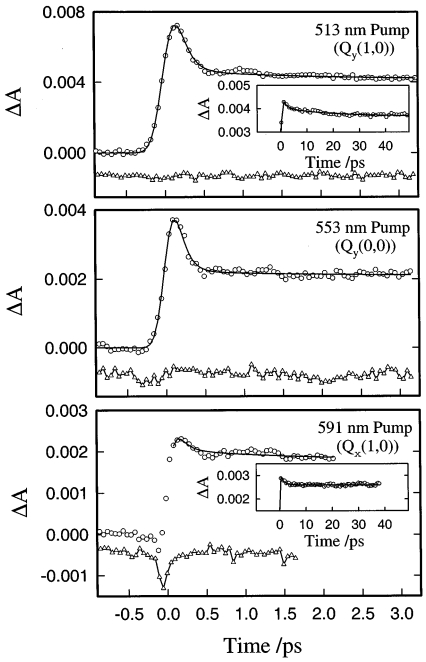


**Figure 7.** Femtosecond transient absorbance of $H_2TPP$ at 657 nm for three pump wavelengths: 513 nm (in benzene, $A_{513} = 0.6$); 553 nm (in benzene-$d_6$, $A_{553} = 0.18$); 591 nm (in benzene, $A_{591} = 0.18$ for the main figure and 0.5 for the inset). Pump energy was 2.0 $\mu$J/pulse. Long time scans in the insets were in 5 mm cells at lower time resolution. The signal when the sample cell was replaced by a cell with solvent alone is shown below each short time scan. The time axes in this figure were not calibrated for the use of different cells for sample and solvent scans. Solid lines are fits of the experimental data using a common set of lifetimes (see text). The rise of the 591 nm transient was not included in the fitting because of clear distortion caused by the solvent response.

conversion. Here, however, although the solvent response causes a distortion in the rising edge of the signal (which was therefore excluded from the fit), its sign eliminates the possibility that the femtosecond component is attributable to the solvent only. The transient in the main figure is fit with 110 fs and 1.4 ps components, the latter of which can be very clearly seen in the inset.

## 4. Discussion

The first conclusion that we can draw from our data is that the flow of population from the Soret band to levels of the Q band takes place very rapidly. With the benzene Raman signal and measurements of zinc tetraphenylporphyrin fluorescence under identical conditions serving to establish both the width and position of the temporal response function of the up-conversion apparatus, our measurements of 435 nm fluorescence place an upper limit on the Soret lifetime of ~50 fs. This ultrafast relaxation is further evidenced by the fact that fluorescence across the Q band emission spectrum fits well with no initial rise time, while under our conditions, a rise time of more than 100 fs should be detectable. This fluorescence can only reasonably be interpreted as Q band emission, so its immediate rise is independent confirmation of a short Soret band lifetime, assuming homogeneous kinetics.

Further evidence of a very fast Soret relaxation is provided by the fact that data for $Q_y$ band excitation matches to a high degree that for Soret excitation, as shown in Figures 4, 5, and 7. The similarity of rates and amplitudes in the transient behavior requires that the populations being probed in each case undergo nearly identical spectral evolution of absorption and emission properties, from the earliest detectable times. This would be highly unlikely unless the same states and the same processes are involved. Because the $Q_y$ excitations do not produce significant population of the Soret, it follows that, when the latter is excited, it must be depopulated faster than we can resolve.

A lifetime of less than 50 fs for the Soret band is in good accord with the estimate based on fluorescence yield and also appears consistent with the measurement and interpretation of Fong and co-workers,[22] who reported an estimated internal conversion (IC) rate of tens of femtoseconds following excitation at 398 nm in chloroform. In a subsequent publication presenting further analysis of the data,[23] however, a longer IC rate of ~200 fs is derived, a value well outside the range established by the current measurements in benzene solution.

One factor that may be invoked in the very significant acceleration of Soret band relaxation in $H_2TPP$ compared to that in ZnTPP,[7,13,32,33] as well as in other metalloporphyrins,[33] is the reduced energy gap between electronic states caused by the Q band splitting in $H_2TPP$; note that the splitting is due to a reduction in molecular symmetry. According to the energy-gap law, the rate decreases exponentially with increasing energy gap. This relation has been invoked in previous analyses of the variation in Soret lifetimes with environment.[33,34] The energy gap between B(0,0) and $Q_y$(0,0) of $H_2TPP$ in benzene is ~5650 $cm^{-1}$, while in ZnTPP the B(0,0)−Q(0,0) gap is ~6670 $cm^{-1}$. If the correlations of energy gap vs rate, which are plotted in refs 33 and 34, are extrapolated to smaller energy gap, both show that a femtosecond rate would be expected for an energy gap of 5650 $cm^{-1}$, although they differ by several orders of magnitude in the precise value predicted. Symmetry reduction, which increases the density of vibronic states in the accessible bath, may also play a role in reducing the lifetime of $H_2TPP$ relative to metalloporphyrins.

However, comparison with the results of measurements of line widths of supersonically cooled $H_2TPP$ by fluorescence excitation[26] suggests that vibronic coupling is an important factor in the ultrafast relaxation of the $H_2TPP$ Soret band in solution. The line widths of vibronic bands assigned to low-energy vibrational modes (excess energy ≤ ~100 $cm^{-1}$) in the Soret state manifold were as narrow as 3 $cm^{-1}$. Using the $Q_x$ line width of 2 $cm^{-1}$ measured in the same study as the contribution of rotational broadening, the authors inferred a Soret lifetime broadening of ~1 $cm^{-1}$ and thus a lifetime of at least 5 ps. Even if the entire 3 $cm^{-1}$ were attributable to lifetime broadening, these measurements show conclusively that the gas-phase lifetime of the vibronic state measured cannot be shorter than about 1.8 ps. For comparison, the same assumption for ZnTPP measurements, also from ref 26, gives a line-width-imposed lower limit of 900 fs for the gas-phase lifetime of the Soret electronic origin, which shows no discrepancy with solution phase lifetime measurements[7,13,32,33] for the dominant Soret emission (emission from the state designated as $S_2$ in ref 13).

Given the assigned electronic origins of 398.2 and 530.0 nm for the $H_2TPP$ Soret and $Q_y$ states in the gas phase, the electronic state energy gap is ~6240 $cm^{-1}$. This value is 10% larger than that of $H_2TPP$ in solution, so a lengthened gas-phase lifetime is qualitatively in agreement with the energy-gap effect, but quantitatively, the energy-gap difference is far too small to account for the dramatic lifetime change. Indeed, the energy-gap increase from solution to gas phase is even greater for ZnTPP, without any indication of a related lifetime increase. Thus, we conclude that the lifetime of the Soret origin remains longer in $H_2TPP$ than in ZnTPP, contrary to expectations from energy-gap and symmetry arguments alone.

This being the case, the discrepancy between solution and jet-cooled, gas-phase Soret lifetimes of $H_2TPP$ must have its origin in the vibrational excitation that is present in the solution-phase experiment. That the Soret lifetime may depend dramatically on vibrational energy is suggested by examination of the $H_2TPP$ excitation spectrum in Figure 7 of ref 26. Within 100 $cm^{-1}$ of the assigned Soret electronic origin, a broad absorption continuum appears to be building up, while the linelike structure at excess energies greater than 100 $cm^{-1}$ (in the limited range shown) appears more diffuse than the lower-energy structure from which the lifetime lower limit of 5 ps was derived. Such behavior is characteristic of interelectronic coupling that is strongly promoted by vibrational excitation, resulting in a rapid acceleration of the internal conversion rate as a function of excess vibrational energy.

In solution at room temperature, molecules with low-energy vibrational modes (such as those associated with phenyl group motions in $H_2TPP$) will carry an average of 200 $cm^{-1}$ of excess energy per mode, so vibrational averaging must be considered when comparing solution-phase and gas-phase dynamics. In our experiments, the laser at 397 nm deposits 1300 $cm^{-1}$ of additional excess energy in the Soret band, and internal conversion occurs before this energy can be dissipated to the solvent. Thus, our measurement probes only significantly excited levels of the Soret band. The lifetime upper limit of 50 fs that is placed on these levels by our time-resolved measurements is consistent with the molecular beam study if the lifetime is strongly dependent on vibrational energy.

Accepting the evidence of the gas-phase line widths that the Soret origin lifetime of $H_2TPP$ is longer than that of ZnTPP, we conclude not only that vibrational excitation has a dramatic accelerating effect on the Soret decay rate of $H_2TPP$ but that no such effect occurs in ZnTPP. It is possible that the reason for this difference is associated with the effect of the metal center on porphyrin rigidity and torsional mode frequencies at the molecular core. The difference in limiting lifetimes with sufficient vibrational excitation (femtosecond for $H_2TPP$, picosecond for ZnTPP) may still be reasonably ascribable in large part to energy-gap and symmetry effects.

Because the lifetime of the Soret band of $H_2TPP$ in benzene is too short to be resolved in our measurements, the lifetimes that are measured must correspond to evolution of population within the Q band. The fourth component, which accounts for all transient behavior at times longer than 100 ps, is evidently and consistently ascribable to dynamics of the equilibrated $Q_x$ state (and equilibrated $T_1$ in transient absorption), for which virtually all molecules are in the ground level of the Franck−Condon active, and thus spectrally relevant, vibrational mode. Therefore, the three distinct ultrafast processes observed on the femtosecond and picosecond time scale are steps between the initially prepared distribution of Q state levels and equilibrated $Q_x$.

An important factor in establishing the nature of these processes is the time dependence of the fluorescence spectral profile. From consideration of the absorption and fluorescence[18,28] spectra, emission from the levels of the $Q_y$ state with 0 and 1 quantum in the Franck−Condon active mode is expected to lie predominantly between 514 and 600 nm. However, the fluorescence spectrum following $Q_y(1,0)$ (514 nm) excitation, of which the evolution above 570 nm is represented in the inset to Figure 4, is dominated by emission at 645 nm even in the first 200 fs. The substantial intensity around 600 nm may have contributions of $Q_y$ emission, but the fact that $Q_x$ is already strong and shows no rise corresponding to the 600 nm decay indicates that $Q_y-Q_x$ IC, like Soret relaxation, is unresolvably short and, therefore, that the three resolvable ultrafast processes correspond to three distinguishable steps in $Q_x$ relaxation.

In further support of this conclusion, we note that the jet-cooled gas-phase excitation spectra of ref 26, which show sharp, well-resolved structure in $Q_x$ and at low energies in the Soret band, show only a 120 $cm^{-1}$ wide unresolved band assigned to the $Q_y$ origin. Assuming that the $Q_y$ vibrational structure is similar to that of $Q_x$ (three strong lines with 20 $cm^{-1}$ separations), the observed band can be reproduced only if each line is broadened to a width of ~100 $cm^{-1}$, corresponding to 50 fs lifetimes. If this is the case, it is notable that the $Q_y-Q_x$ coupling is as much as 100 times that of B−Q in the absence of vibrational excitation.

That the observed transient behavior in emission and absorption shows little dependence on whether the $Q_y(1,0)$ or $Q_y(0,0)$ band is excited is found to be easily consistent with the above conclusion that all observed dynamics take place in the $Q_x$ state after IC in <100 fs. Additionally, the data of Figure 5 and particularly Figure 7 show that even direct excitation of $Q_x(1,0)$ gives rise to two fast dynamic processes comparable to those for Soret and $Q_y$ excitation.

The question that now remains is the following: To what physical processes in the $Q_x$ state do the three observed lifetimes correspond? The longest has the expected characteristics of vibrational relaxation representing thermal equilibration with the solvent. For both Soret and $Q_y$ excitation, the $Q_x(0,0)$ fluorescence peak narrows in this process, because the component appears as a rise at the band maximum and as a decay in both the red and blue wings of the band. The time scale is similar to those assigned to vibrational cooling in other femtosecond studies of tetraphenylporphyrins.[3,4,13,35] The trend in the amplitude of this component with the excitation energy is also consistent with this assignment; for a given detection, it is generally largest when exciting the Soret band and diminishes as the disequilibrating impulse of imparted excess vibrational energy decreases, becoming undetectable when exciting $Q_x(1,0)$.

The shortest component (100−200 fs lifetime) is seen for all excitations with substantial amplitude. It appears in fluorescence as a decay on the blue side of the emission spectrum and is absent at the fluorescence maximum and longer wavelengths. (Only in the 700 nm fluorescence for Soret band excitation is a rise suggested, but the data are inconclusive.) The time scale and spectral characteristics suggest an intramolecular vibrational energy redistribution (IVR) process, in which energy that is initially coherently deposited in a subset of the vibrational phase space spreads to a larger set of states at equal total energy under the influence of intramolecular mode couplings.

In this process, the initially formed coherent superposition of excited eigenstates (wave packet) dephases because of the small but finite energy spread among the constituent states. The dephasing rate is determined by the nature of the impulse that creates the superposition, the coupling among states, and the bandwidth of the probe process. When the superposition is directly formed by pulsed laser excitation, IVR will be bandwidth-limited to occur on the time scale of the pulse width, in this case ~100 fs, or slower. We measure lifetimes of this order in transient absorption for Q band excitation and somewhat slower for other experiments. Changes with excitation pathway (Soret, $Q_y$, or $Q_x$) may reflect the different nature of the $Q_x$ superposition state formation, but differences are also seen when exciting the same $Q_y$ absorption bands and using different detection methods (e.g., Figure 5 vs Figure 7), so no definitive conclusion on the effect of excitation can be reached.

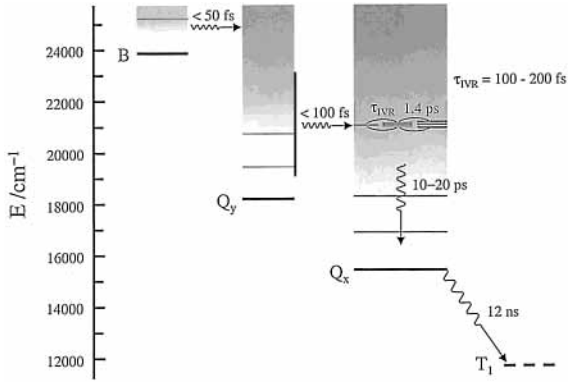


**Figure 8.** Schematic diagram of the energy relaxation dynamics of $H_2TPP$ in benzene. The solid horizontal lines are located at the energies of bands in the absorption spectrum and are identified with Franck−Condon active vibrational levels of the $Q_x$, $Q_y$, and B electronic states. The approximate energy of the triplet, $T_1$, is indicated by a dashed line. See text for details of the dynamics.

The component of intermediate lifetime ($\tau_2 = 1.4$ ps) has characteristics similar to those of the fast component, although the amplitudes are smaller. It's clear appearance in transient absorption for $Q_x(1,0)$ excitation argues against associating this component with conventional vibrational cooling. With only a small surplus of vibrational energy above the thermal content, equilibration from $Q_x(1,0)$ would not be expected to occur faster than it does from higher excitation energies. Therefore, a process distinct from cooling appears to be indicated.

One possibility is that this process is a solvent-induced vibrational energy redistribution that is caused by elastic or quasi-elastic collisions between the solute and solvent molecules. Such collisions generally have higher cross-section than inelastic collisions, as has been observed in low-pressure gases.[36] By spreading population into regions of the vibrational manifold not strongly coupled to the initial coherent state by the isolated-molecule Hamiltonian, such collisions should produce spectral changes such as those of IVR but on a time scale determined by the elastic collision cross-section. From our measured rates, the elastic cross-section would then be about 10 times larger than the inelastic cross-section.

The pathways and time scales for relaxation of $H_2TPP$ in benzene as discussed in the preceding paragraphs are represented schematically in Figure 8. The IVR and elastic collision processes, which are shown occurring in $Q_x$ when it is populated by IC from higher electronic states, also take place following direct excitation of $Q_x(1,0)$.

## 5. Conclusion

In this paper, we reported our femtosecond study of the relaxation dynamics of free base tetraphenylporphyrin in solution following Soret, $Q_y$, and $Q_x$ band excitation. By using fluorescence up-conversion and pump−probe transient absorption in tandem, the relaxation dynamics of $H_2TPP$ in benzene could be followed in detail via a series of distinct steps to thermal equilibrium in the $Q_x$ state. In our model of the relaxation process, the two higher singlet states undergo internal conversion to $Q_x$ within 100 fs. In the case of Soret excitation, comparison with gas-phase measurements demonstrates that vibrational excitation is key to promoting relaxation from the picosecond time scale to faster than 50 fs. That this promotion does not occur in metalloporphyrins accounts for the long-recognized difference in Soret fluorescence quantum yields between free base and metalloporphyrins. Relaxation in $Q_x$ occurs on three distinct time scales: 100−200 fs for intramolecular vibrational dephasing and 1.4 and 10−20 ps for solvent-induced vibrational relaxation. The faster of the two phases of interaction with the solvent is assigned to elastic collisions, which enhance scrambling of vibrational energy within the solute, while the slower results from energy-exchanging collisions, which lead to thermal equilibrium with the solvent.

**Acknowledgment.** This work was supported by the National Science Foundation (Laboratory for Molecular Sciences). We thank Prof. Fred Anson for discussions that we had in this and related collaborative research.

## References and Notes

(1) Gouterman, M. In *The Porphyrins*; Dolphin, D., Ed.; Academic Press: New York, 1978; Vol. 3, p 1.
(2) Kalyanasundaram, K. *Photochemistry of Polypyridine and Porphyrin Complexes*; Academic Press: London, 1992.
(3) Rodriguez, J.; Holten, D. *J. Chem. Phys.* **1989**, *91*, 3525.
(4) Rodriguez, J.; Kirmaier, C.; Holten, D. *J. Chem. Phys.* **1991**, *94*, 6020.
(5) Gentemann, S.; Nelson, N. Y.; Jaquinod, L.; Nurco, D. J.; Leung, S. H.; Medforth, C. J.; Smith, K. M.; Fajer, J.; Holten, D. *J. Phys. Chem. B* **1997**, *101*, 1247 and references therein.
(6) Akimoto, S.; Yamazaki, T.; Yamazaki, I.; Osuka, A. *Chem. Phys. Lett.* **1999**, *309*, 177.
(7) Mataga, N.; Shibata, Y.; Chosrowjan, H.; Yoshida, N.; Osuka, A. *J. Phys. Chem. A* **2000**, *104*, 4001.
(8) Mizutani, Y.; Kitagawa, T. *J. Mol. Liq.* **2001**, *90*, 233.
(9) Yu, H. Z.; Baskin, J. S.; Steiger, B.; Wan, C. Z.; Anson, F. C.; Zewail, A. H. *Chem. Phys. Lett.* **1998**, *293*, 1.
(10) Yu, H. Z.; Baskin, J. S.; Steiger, B.; Anson, F. C.; Zewail, A. H. *J. Am. Chem. Soc.* **1999**, *121*, 484.
(11) Steiger, B.; Baskin, J. S.; Anson, F. C.; Zewail, A. H. *Angew. Chem., Int. Ed.* **2000**, *39*, 257.
(12) Anson, F. C.; Shi, C.; Steiger, B. *Acc. Chem. Res.* **1997**, *30*, 437.
(13) Yu, H.-Z.; Baskin, S; Zewail, A. H. *J. Phys. Chem. A* **xxxx**, *xxx*, **2002**, *106*, 9845.
(14) Stratt, R. M.; Maroncelli, M. *J. Phys. Chem.* **1996**, *100*, 12981 and references therein.
(15) Dorough, G. D.; Miller, J. R.; Huennekens, F. M. *J. Am. Chem. Soc.* **1951**, *73*, 4315.
(16) Thomas, D. W.; Martell, A. E. *J. Am. Chem. Soc.* **1956**, *78*, 1338.
(17) Edwards, L.; Dolphin, D. H.; Gouterman, M.; Adler, A. D. *J. Mol. Spectrosc.* **1971**, *38*, 16.
(18) Seybold, P. G.; Gouterman, M. *J. Mol. Spectrosc.* **1969**, *31*, 1.
(19) Gradyushko, A. T.; Tsvirko, M. P. *Opt. Spectrosc. (USSR)* **1971**, *31*, 291.
(20) Pekkarinen, L.; Linschitz, H. *J. Am. Chem. Soc.* **1960**, *82*, 2407.
(21) Ohno, O.; Kaizu, Y.; Kobayashi, H. *J. Chem. Phys.* **1985**, *82*, 1779.
(22) Zhong, Q.; Wang, Z.; Liu, Y.; Zhu, Q. H.; Kong, F. A. *J. Chem. Phys.* **1996**, *105*, 5377.
(23) He, Y.; Xiong, Y. J.; Zhu, Q. H.; Kong, F. A. *Acta Phys.-Chim. Sin.* **1999**, *15*, 636.
(24) Kotlo, V. N.; Solovyev, K. N.; Shkirman, S. F. *Izv. Akad. Nauk. SSSR Ser. Fiz.* **1975,** *39*, 1972.
(25) Kurabayashi, Y.; Kikuchi, K.; Kokubun, H.; Kaizu, Y.; Kobayashi, H. *J. Phys. Chem.* **1984**, *88*, 1308.
(26) Even, U.; Magen, J.; Jortner, J.; Friedman, J.; Levanon, H. *J. Chem. Phys.* **1982**, *77*, 4374.
(27) Fiebig, T.; Wan, C.; Kelley, S. O.; Barton, J. K.; Zewail, A. H. *Proc. Natl. Acad. Sci. U.S.A.* **1999**, *96*, 1187.
(28) Quimby, D. J.; Longo, F. R. *J. Am. Chem. Soc.* **1975**, *97*, 5111.
(29) Strickler, S. J.; Berg, R. A. *J. Chem. Phys.* **1962**, *37*, 814.
(30) Bajema, L.; Gouterman, M.; Rose, C. B. *J. Mol. Spectrosc.* **1971**, *39*, 421.
(31) Rodriguez, J.; Kirmaier, C.; Holten, D. *J. Am. Chem. Soc.* **1989**, *111*, 6500.
(32) Gurzadyan, G. G.; Tran-Thi, T.-H.; Gustavsson, T. *J. Chem. Phys.* **1998,** *108*, 385.
(33) Gurzadyan, G. G.; Tran-Thi, T.-H.; Gustavsson, T. *Proc. SPIE−Int. Soc. Opt. Eng.* **2000**, *4060*, 96.
(34) Vacha, M.; Machida, S.; Horie, K. *J. Phys. Chem.* **1995**, *99*, 13163.
(35) Kumble, R.; Palese, S.; Lin, V. S.-Y.; Therien, M. J.; Hochstrasser, R. M. *J. Am. Chem. Soc.* **1998**, *120*, 11489.
(36) Sleva, E. T.; Zewail, A. H. *Chem. Phys. Lett.* **1984**, *110*, 582.